npj | flexible electronics

Article

Published in partnership with Nanjing Tech University

https://doi.org/10.1038/s41528-024-00317-z

Miniaturized all-in-one microneedle device for point of care light therapy

Huiting Zhao[1,2], Xu Wang[1,2], Jiyuan Xiong[1], Guomin Liang[1], Xin Wu[1], Jiyu Xi[1], Yu Zhang[1], Zixi Li[1], Xiaoming Hu[1] ✉ & Zewen Wei[1] ✉

Light therapies have been applied to millions of patients for treating many kinds of diseases, especially superficial ones. Currently, mainstream light therapies utilize the combined effects of photosensitizers and light to either remove disordered tissue or promote the growth of healthy tissue. Adverse effects of light therapy, including metabolic burden caused by circulatory photosensitizer and skin damage induced by high irradiance light, are yet to be addressed. This study provides a Miniaturized all-in-one Light therapy Device (MiLD). All components required for light therapy, including dual-function microneedles, LED array, control circuit, and battery are integrated together to form a miniaturized portable device with 2 cm in length, 1.7 cm in width, 1.2 cm in height, and 3.6 g in weight. The all-in-one design and patch-to-cure operation of MiLD enables the successful demonstration of point-of-care light therapy. Satisfactory therapeutic effects have been verified in mice on both types of light therapy. Meanwhile, transdermally co-delivering both photosensitizer and light in situ fully avoids photosensitizer accumulation in blood and remarkably reduces the irradiance of light, therefore significantly alleviating metabolic burden and light-induced skin damage. Overall, the MiLD lays the technical foundation of point-of-care light therapy with its miniaturized all-in-one design, simple patch-to-cure operation, satisfactory therapeutic effects, and minimum adverse effects.

Light therapies involve exposing patients to light for treating diseases. Since 1903, when ultraviolet light was used for killing superficial bacteria or alleviating the formation of smallpox pustules[1], light therapy has gradually become an effective method for curing multiple diseases[2–5]. Currently, light-mediated therapies have been clinically approved for treating 15 kinds of diseases[6], involving millions of patients per year worldwide. An important milestone during the development of light therapy is the employment of photosensitizer which converts light energy to chemical energy, significantly enhancing the therapeutic effect. For example, the employment of amino-levulinic acid (ALA) improves the therapeutic effect of epidermoid carcinoma by 47%[7], compared with light monotherapy. Hence, multiple photosensitizer-mediated light therapies have been selected as first-line treatments for several diseases. For instance, verteporfin-mediated photodynamic therapy (PDT) has been selected as 1st line treatment for central serous chorioretinopathy[8], while methyl aminolevulinate (MAL)-mediated PDT has been considered as 1st option for treating actinic keratosis[9]. As therapeutic light and photosensitizer are both essential elements of light therapy, precise and efficient delivery of both therapeutic light and photosensitizer into target tissue is the premise for successful photosensitizer-mediated light therapy.

Clinically, most photosensitizers are delivered through intravenous injection, while therapeutic light is directly applied to the target tissue[10,11]. Unfortunately, neither intravenous injection of photosensitizer nor direct illumination can be considered an ideal delivery method. Intravenous photosensitizer injection will inevitably accumulate photosensitizer in the circulatory system, consequently burdening the metabolic system and harming healthy tissue[12,13]. Moreover, uncontrolled activation of circulatory photosensitizer by ambient light leads to the generation of undesired cytotoxic reactive oxygen species (ROS), inducing damage to the skin[14] or eyes[15]. As a result, patients must be strictly shielded from daylight for up to 4–6 weeks after treatment[16], which is quite inconvenient and reduces the applicability of light therapy. On the other side, direct illumination requires relatively higher light irradiance (usually up to 150–500 mW cm^{-2})[17–19] to compensate for energy loss in the stratum corneum, most likely causing immediate pain[20] and tissue damage[21,22]. Moreover, generating well-controlled therapeutic light with high irradiance requires specially designed apparatus which usually are bulky and costly, limiting the availability of equipment to central hospitals[23,24]. Considering the fact that typical light therapies usually involve multiple times of treatments, lasting for 10–40 months[25,26]. The inconvenience of frequent commuting to the

[1]School of Medical Technology, Beijing Institute of Technology, Beijing 100081, China. [2]These authors contributed equally: Huiting Zhao, Xu Wang.
✉e-mail: bithxm@bit.edu.cn; weizewen@bit.edu.cn

hospital compromises patient compliance. These adverse effects, including photosensitizer-involved metabolic burden and therapeutic light-induced tissue damage, can be considered as necessary prices for treating deep organ diseases. On the other hand, for superficial diseases, such prices can be avoided by alternative methods, for instance, transdermal delivery.

Currently, methods for transdermally delivering either photosensitizer or therapeutic light into target tissue have been explored. For transdermally delivering photosensitizer, both chemical[27–29] and physical[30,31] assisted methods have been developed. Taking actinic keratosis as an example, satisfactory therapeutic effects of PDT are realized by physical-assisted transdermal photosensitizer delivery methods, including iontophoresis-mediated delivery of MAL (with a complete recovery rate of 88.7%)[32] and microneedle-mediated delivery of ALA (with a complete recovery rate of 76%)[33]. Besides, chemical-assisted methods have also been validated. For example, transfersome-mediated delivery of indocyanine green results in a complete recovery rate of 80%[34] for treating basal cell carcinoma. Differing from transdermally delivering photosensitizer, which has already been clinically verified, transdermally delivering therapeutic light is still in the early stages of exploration. Existing proof-of-concept studies mainly focus on utilizing biodegradable polymers, including poly(lactic acid) (PLA) and poly(lactide-co-glycolide) (PLGA), to form waveguides for guiding therapeutic light to penetrate the skin surface[35,36]. Nevertheless, the clinical effectiveness of transdermally delivering therapeutic light for treating superficial disease has not yet been confirmed. Moreover, the concept of transdermal delivering both photosensitizer and guiding therapeutic light simultaneously has also been raised[37]. Despite that transdermal delivery of either photosensitizer or therapeutic light has respectively been verified as beneficial advances for improving light therapy, transdermal co-delivery of photosensitizer and therapeutic light by a full-function portable device to treat superficial diseases is yet to be realized.

To address the feedbacks of the intravenous photosensitizer administration, the direct illumination, and the high-level equipment requirements, a Miniaturized all-in-one Light therapy Device (MiLD) based on dual-function microneedles has been developed. The dual-function microneedles which consist of dissolvable tips for delivering photosensitizer and transparent needle bodies for guiding therapeutic light have been fabricated to facilitate transdermally co-delivering photosensitizer and therapeutic light into target tissue, ensuring efficient light therapy. The miniaturized dimension, battery-powered all-in-one design, and wireless remote control of MiLD enable a simple patch-to-cure operation, therefore relieving patients from the inconvenience of repetitive intra-hospital treatments, and more importantly, laying the foundation of point-of-care light therapy.

Results and discussion

Miniaturized All-in-One Light Therapy Device (MiLD)

A Miniaturized all-in-one Light therapy Device (MiLD) has been developed to facilitate efficient point-of-care light therapy with minimum adverse effects. Figure 1a schemes a simple patch-to-cure operation for treating superficial diseases by MiLD. The MiLD can be directly patched to the skin surface. Dual-function microneedles penetrate the stratum corneum with minimum damage. After patching on the skin and maintaining for several minutes, the tips (marked red in Fig. 1a) of dual-function microneedles are dissolved to deliver loaded photosensitizer into the target tissue, leaving transparent needle bodies to guide therapeutic light (marked glow green in Fig. 1a) into the same tissue area. Then the MiLD is remotely controlled through a Bluetooth® wireless link. A software (Supplementary Fig. 1) is developed to manipulate MiLD to emit therapeutic light with proper irradiance and duration for treating diverse diseases. Differing from typical intra-hospital light therapy instruments (>48.5 cm in length, 22 cm in width, 40.5 cm in height, >19 kg in weight), the battery-powered MiLD (2 cm in length, 1.7 cm in width, 1.2 cm in height and 3.6 g in weight) is a fully portable device (Supplementary Fig. 2). Meanwhile, the employment of MiLD avoids laborious and time-consuming intra-hospital treatment, and more importantly, prevents patients from undergoing hard-to-endure post-treatment shading procedures (Supplementary Fig. 3). Hence, the MiLD throws light on point-of-care light therapy. Figure 1b schemes the MiLD design, while Fig. 1c shows the dimensions of fabricated MiLD (2 cm in length, 1.7 cm in width, 1.2 cm in height, and 3.6 g in weight). Figure 1d illustrates the therapeutic light emitted by MiLD under battery-powered and remote control. A schematic diagram (Fig. 1e) exhibits the structure of MiLD. From bottom to top, the MiLD consists of 5 layers: a dual-function microneedle array for co-delivering photosensitizer and therapeutic light in a transdermal manner; a light emitting diode (LED) light source for generating therapeutic light; a graphene membrane for dissipating heat generated by both control module and LED; a control module for remotely regulating LED to emit therapeutic light; a lithium battery for powering the MiLD. Figure 1f shows the photo of the dual-function microneedle array consisting of 400 microneedles with a spacing of 500 μm. Each microneedle is made up of a photosensitizer-loaded sodium hyaluronate (HA) tip (red portion) and a transparent polyvinyl alcohol (PVA) needle body. Scanning electron microscope (SEM) (Fig. 1g) photo displays the profile of microneedles. A close-up view of a single microneedle (Fig. 1h) shows its two-stage structure. After placing in living tissue for several minutes, HA tips are dissolved to release loaded photosensitizer. Figure 1i shows the PVA needle bodies, which are transparent (Fig. 1j), thus enabling transdermal light-guiding. Figure 1k shows the LED light source coupled with microneedle array. LED is selected as the light source as it bears the advantages of high energy efficiency ratio and ideal narrowband wavelength. LEDs are welded to polyimide (PI) circuit board as an array to form the light source. Figure 1l shows the illumination of LED light source through microneedle light-guide. Since the LEDs and the needle bodies are tightly coupled, the light scattering and refraction are minimized. Therefore, very little light leaks through the spacing between adjacent needles and the edge of the MiLD. The wavelength of therapeutic light is 525 nm in this study and the emission spectroscopy of the LED array is measured (Supplementary Fig. 4). The wavelength can be easily varied by replacing LEDs to meet the requirements of other light therapies. The heat generated by LED and circuit board is rapidly dissipated by a graphene membrane to avoid skin burn. Our study uses a graphene membrane as a heat management strategy to dissipate heat produced by the point-of-care light therapy device. The heat-dissipating effect of graphene membrane is quantified (Supplementary Fig. 5). It is demonstrated that embedding graphene membrane remarkably lowers the temperature by 9.36–18.10 °C. Moreover, the graphene membrane also helps to maintain a constant temperature during the whole operation duration of MiLD. For instance, the MiLD maintains a temperature range of 35.6–36.3 °C while the light intensity is 20 mW cm^{-2} (Supplementary Fig. 6). Figure 1m shows a circuit board acting as the control module of MiLD. Figure 1n shows the circuit diagram. Control commands are received through Bluetooth® wireless link and then processed by microcontroller unit (MCU) to drive the LED. Like light wavelength, the adjustable range of light irradiance can also be modified according to other demands by simply replacing the LED and its driver module. Figure 1o outlines the fabrication process of MiLD. Briefly, a copper microneedle master is prepared using a 5-axis machine tool. Polydimethylsiloxane (PDMS) is poured onto the master and cured at 80 °C to form the microneedle mold. Supplementary Fig. 7 shows the PDMS microneedle mold with arrayed cavities. Photosensitizer-loaded HA solution is then poured onto the PDMS mold and placed in a vacuum environment (−0.9 bar) for 30 min to creat the tips. Excessive photosensitizer-HA mixture is cleared. PVA solution is poured onto PDMS mold and placed in the same vacuum environment for 10 min to obtain the microneedle bodies. The PVA has not yet begun to solidify at this moment. The LED array is tightly attached to PVA solution and maintained there until the PVA is fully solidified at room temperature for 48 h. The base width and height of transparent needle body are 300 and 700 μm, respectively. The height of needle tip is 100 μm. Finally, the LED-coupled microneedle array is stripped from the mold and assembled with graphene membrane, control module, and battery in consequence to form the MiLD.

The performance of MiLD in transdermally co-delivering photosensitizer and therapeutic light by remote commands is investigated. As

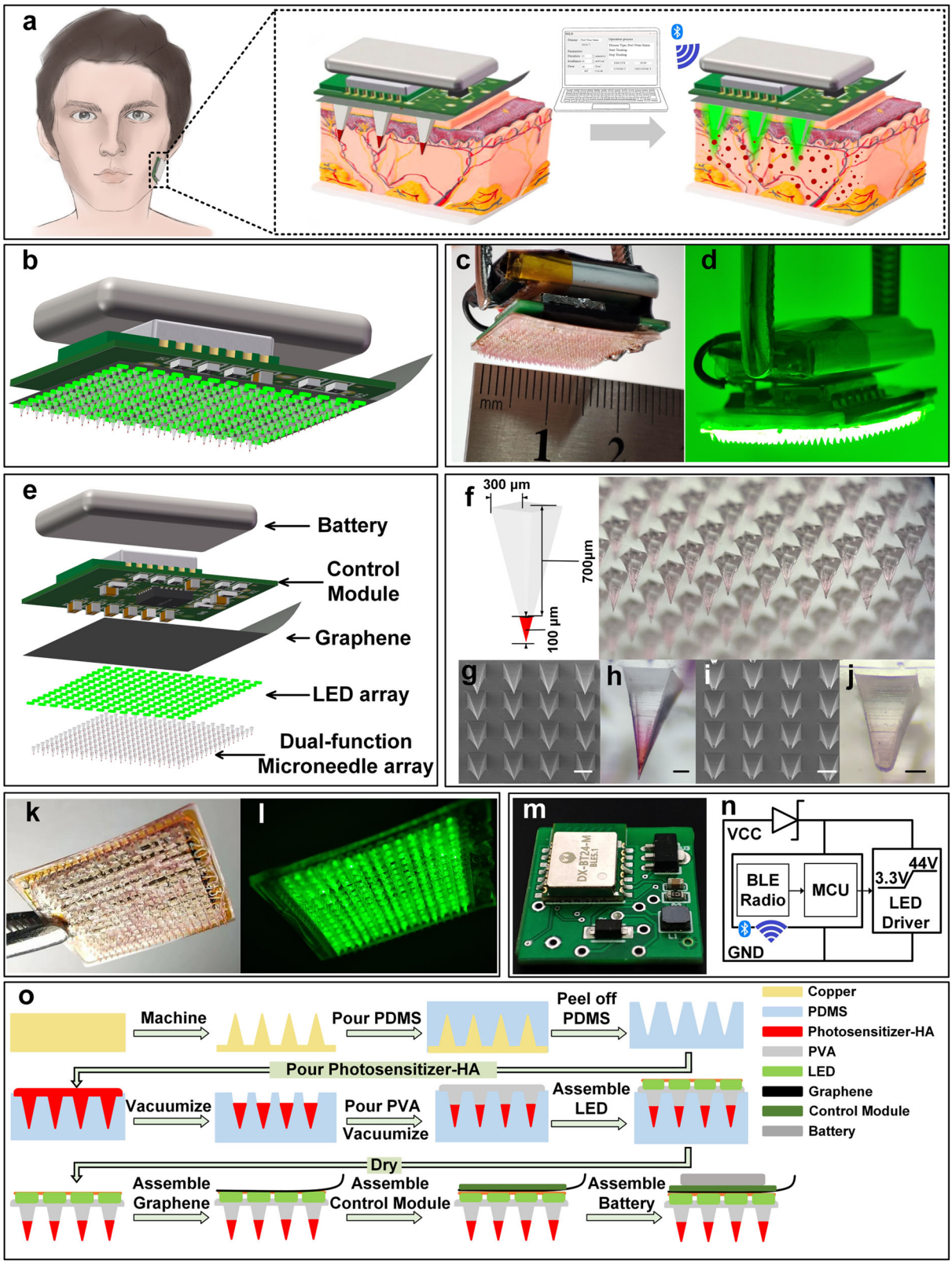

Fig. 1 | Light therapy based on the Miniaturized all-in-one Light therapy Device (MiLD) for treating superficial diseases. a Scheme of utilizing MiLD-mediated light therapy to treat superficial diseases. The battery-powered MiLD was patched to the target tissue and an enlarged view illustrated the therapeutic procedures using MiLD. **b** Schematic diagram and (**c**) photo of the MiLD. **d** The MiLD emitting therapeutic light at 525 nm. **e** Exploded view of the MiLD including a dual-function microneedle array, LED light source, graphene membrane, control module, and battery. **f** Photo of a dual-function microneedle array. **g** SEM of microneedles (scale bar: 300 μm). **h** Photo of a single microneedle (scale bar: 100 μm). **i** SEM of microneedles after tips dissolved (scale bar: 300 μm). **j** Photo of a single PVA light-guide (scale bar: 100 μm). **k** Photo of a LED-coupled microneedle array. **l** LED illumination through microneedle light-guide. **m** Photo of the circuit module. **n** Circuit diagram of the MiLD for wireless-controlled therapeutic light emission. **o** The preparation process of the MiLD.

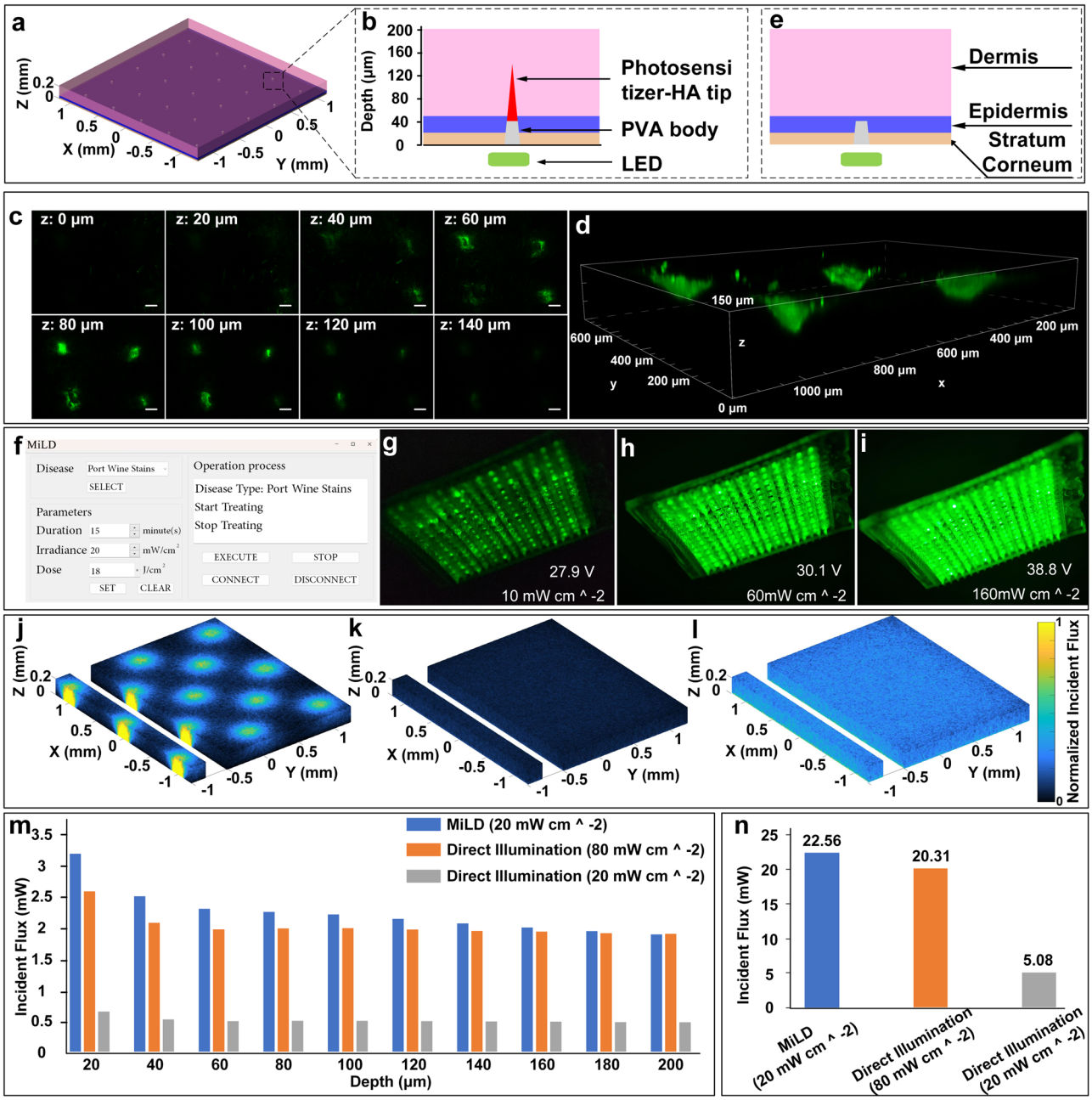

Fig. 2 | Characterization of the MiLD. a Numerical analysis model of the MiLD inserted into mouse skin. **b** Schematic cross-section of LED-coupled microneedle pierced into the skin. **c** Confocal fluorescent images of skin from the skin surface (marked as 0 μm) to 140 μm beneath the skin (scale bar: 100 μm). **d** 3D reconstruction of microchannel created by FITC-labeled microneedles insertion. **e** Cross-section view of a LED-coupled light-guiding body within the skin. **f** Photo of the control software. **g–i** Illumination of LED light source coupled with microneedles light-guides at irradiance from 10 mW cm^{-2} to 160 mW cm^{-2}. Monte Carlo simulation of incident light flux in mice skin under (**j**) MiLD-mediated illumination at 20 mW cm^{-2} irradiance (**k**) direct illumination at 20 mW cm^{-2} irradiance and (**l**) direct illumination at 80 mW cm^{-2} irradiance. **m** Optical power delivered to skin tissue at different depths intervals, 20 μm each, under three illumination conditions. **n** Total optical power in skin tissue.

shown in Fig. 2a. a Monte Carlo Analysis model is established to sketch the scenario of MiLD penetrating mouse skin. An enlarged cross-section view (Fig. 2b) shows the skin anatomy consisting of three layers: the stratum corneum (exhibited as a yellow layer, 20 μm thick), the epidermis (exhibited as a blue layer, 30 μm thick), and the dermis (exhibited as a pink layer, 150 μm thick). LED-coupled microneedle penetrates the stratum corneum, enabling the photosensitizer-loaded tip (marked red in Fig. 2b) to enter the dermis. The mechanical properties and puncture capabilities of microneedle are investigated. The force-displacement curve illustrates that the compression strength of the microneedle is 24.178 N. Moreover, the microneedle arrays are capable of penetrating mouse skin for transdermal delivery of photosensitizer (Supplementary Fig. 8). To test the depth of microneedles insertion, fluorescein isothiocyanate (FITC) is encapsulated in HA-tips. After microneedles insertion, the mouse skin is fluorescently imaged by confocal microscopy (Fig. 2c). The reconstructed 3D profile (Fig. 2d) reveals the pathway of microneedles insertion. The experimental results demonstrate that the depth of microneedles insertion is 140 μm under a gentle manual punching process. Such a depth reaches a balance between successful penetration of stratum corneum and minimized tissue damage. The insertion depth can be adjusted according to demands by varying the punching strength. As shown in Fig. 2e, after maintaining the microneedle in the target tissue for 5 min, the photosensitizer/HA tip is fully dissolved,

leaving a transparent needle body. The dissolving process of HA needle tips is evaluated by employing 3% agarose gel as artificial tissue (Supplementary Fig. 9).

The LED light source is activated to generate therapeutic light. The irradiance and duration of therapeutic light are set in control software (Fig. 2f). The most commonly used parameter combinations for treating different diseases are pre-set in the software to realize a user-friendly operation which is a premise for point-of-care light therapy. By pulse width modulation (PWM), the irradiance of the LED light source enhances from 10 mW cm^{-2} to 160 mW cm^{-2}, as the driving voltage increases from 27.9 to 38.8 V (Fig. 2g–i). Using the depth of microneedles insertion as the reference, the light-guiding efficiency is calculated by Monte Carlo simulation, which is a widely accepted numerical method for optical simulation. Figure 2j shows the distribution of incident flux inside the skin while the irradiance of microneedles-mediated illumination is 20 mW cm^{-2}. The microneedles act as light-guides to direct therapeutic light into the skin tissue. In comparison, while directly illuminating the skin surface at 20 mW cm^{-2} irradiance without the participation of microneedles, the incident flux inside the skin is much lower (Fig. 2k), as a large part of therapeutic light is blocked by the stratum corneum. To compensate for the therapeutic light loss in the stratum corneum, the irradiance should be enhanced to 80 mW cm^{-2} to generate a light distribution in skin tissue similar to that of microneedles-mediated illumination at 20 mW cm^{-2} irradiance (Fig. 2l). To predict the total light energy for light therapy, the incident flux values at different depths from the skin surface are calculated. As shown in Fig. 2m, from the skin surface to 200 μm beneath the skin, the microneedles-mediated illumination at 20 mW cm^{-2} irradiance generates incident flux similar to that of direct illumination at 80 mW cm^{-2} irradiance. Both produce significantly higher incident flux than direct illumination at 20 mW cm^{-2} irradiance. The total incident flux in tissue from the skin surface to 200 μm beneath the skin is also added. As shown in Fig. 2n, the microneedles-mediated illumination at 20 mW cm^{-2} irradiance and the direct illumination at 80 mW cm^{-2} irradiance produce almost equal incident flux beneath the stratum corneum (22.56 mW and 20.31 mW). In contrast, the total incident flux of direct illumination at 20 mW cm^{-2} irradiance is only 5.08 mW. These results suggest that the microneedle light-guide avoids light scattering and absorption in the stratum corneum and therefore significantly increases effective incident flux in tissue beneath the stratum corneum. As a result, the employment of microneedle light-guide may remarkably reduce the required irradiance for light therapy, and corresponding alleviating the therapeutic light-induced tissue damage.

MiLD mediated light therapy for removing disordered tissue

The therapeutic effect of light therapy is either removing disordered tissue or promoting the growth of healthy tissue. To validate the MiLD, the effectiveness of MiLD-mediated light therapies in removing disordered tissue or promoting the growth of healthy tissue are both examined. Photodynamic therapy (PDT), in which photosensitizers are activated by therapeutic light to generate cytotoxic reactive oxygen species (ROS), is currently a commonly used light therapy for removing disordered tissue, including tumors, disordered skin or malformed vessels. Compared with lethal malignant tumors, non-fatal skin diseases have a lower tolerance for adverse effects of light therapy and place a higher requirement on the convenience of operation. Therefore, a typical skin disease, port wine stains (PWS) is selected to test the performance of MiLD. PWS is a skin vascular malformation, affecting approximately 22 million patients worldwide[38]. The essence of treating PWS by PDT is to destroy malformed vessels with minimum damage to normal skin. Figure 3a schemes a proof-of-concept PDT for treating PWS in mouse, involving 3 main steps: Step 1, a MiLD is prepared and inserted into mouse skin; Step 2, after inserting the skin with MiLD and maintaining for 5 min, the needle tips are fully dissolved to release the photosensitizer to the tissue; Step 3, following a 30-min waiting for photosensitizer diffusion within the tissue, the MiLD is remotely operated by a control software to emit therapeutic light at a wavelength of 525 nm. The needle bodies act as light-guides for delivering therapeutic light into the skin. Skin vessels in the treated area are imaged daily for 5 days post-treatment to evaluate the effectiveness of MiLD-mediated PDT employing light-induced ROS to damage malformed vessels. As shown in Fig. 3b, skin vessels are imaged via a dorsal skin-fold window chamber (DSWC), which is a standard tool for monitoring superficial vascular diseases. Hemoporfin (HMME), which is an accepted photosensitizer for treating PWS, is used in this study. The mice are divided into five groups: Group 1 is treated with HMME-loaded MiLD (0.75 μg HMME), without therapeutic light, for evaluating the effects of HMME-loaded MiLD without applying therapeutic light. Group 2 is treated with unloaded MiLD, emitting therapeutic light at an irradiance of 20 mW cm^{-2}, for evaluating the effects of MiLD applying therapeutic light alone. Group 3 is treated with intravenously injected (IV) HMME (300 μg), followed by direct illumination at an irradiance of 20 mW cm^{-2}, for evaluating the effects of traditional PDT with relatively lower light irradiance. Group 4 is treated with intravenously injected (IV) HMME (300 μg), followed by direct illumination at an irradiance of 80 mW cm^{-2}, which is commonly used in clinical practice. This group serves as the positive control for confirming the validity of the experimental operation procedures. Group 5 is treated with HMME-loaded MiLD (0.75 μg HMME) emitting therapeutic light at an irradiance of 20 mW cm^{-2} for validating the effectiveness of MiLD-mediated PDT. The intuitive results obtained from the skin vascular images are presented in Fig. 3b. No markable vascular damage is found in Groups 1, 2, and 3, while varying degrees of vascular disappearance are observed in Groups 4 and 5. To further quantify the vascular damage, the original vascular images are converted to binary images, and an algorithm (described in detail in Supplementary Fig. 10) is developed to calculate the vascular areas. As shown in Fig. 3c, the vascular area initially increases and then stabilizes in Groups 1, 2, and 3, reaching about 159%, 145%, and 139% of the initial area on the 5th day after PDT, respectively. This implies that the presence of photosensitizer or therapeutic light alone does not lead to vascular injury. Moreover, the irradiance of 20 mW cm^{-2} in PDT is also insufficient to induce vascular damage due to inadequate levels of ROS. Only when the irradiance is increased to 80 mW cm^{-2} (Group 4), can the combined action of intravenously injected photosensitizer and therapeutic light effectively damage vessels (Supplementary Fig. 11). The vascular area in Group 4 is about 8% of the initial value on the 5th day after PDT. Similarly, the HMME-loaded MiLD (Group 5), also shows a satisfactory therapeutic effectiveness but with a lower light irradiance (20 mW cm^{-2}) and HMME dose (0.75 μg), as the vascular area is about 11% of the initial value in Group 5. In the mouse model, the MiLD-mediated PDT and traditional PDT have similar healing times. However, traditional PDT requires high light irradiance, which may induce pain or even scarring. Meanwhile, the strict light shielding in traditional PDT also reduces patient comfort and compliance.

Traditional PDT involves high-irradiance therapeutic light, which may induce not only pain/scarring, but also histological changes and tissue inflammation due to high irradiance illumination-induced overheating. As expected, the MiLD significantly decreases the light irradiance of PDT from 80 to 20 mW cm^{-2}. To assess the advantages of reduced irradiance, the histological changes and inflammation are determined by hematoxylin and eosin (H&E) staining of the mouse skin. Compared with healthy skin (Fig. 3d), direct illumination (80 mW cm^{-2}) changes the tissue morphology (Fig. 3e), as the epidermis is thickened and dermal fibers are broken. Moreover, the inflammatory response is also observed. As shown in Fig. 3e, the dermis, sebaceous glands, and hair follicles are infiltrated with inflammatory cells, which are stained by blue hematoxylin. Both histological changes and inflammation are significantly alleviated in the mouse skin treated with MiLD (20 mW cm^{-2}) (Fig. 3f). Excessive light exposure often leads to an overheating of the skin tissue, which may also result in abnormal gene expression, mainly involving the inflammation-related IL1 upregulation. To further investigate the benefits of reduced irradiance at the molecular level, the expressions of IL1 transcripts in mice skin are determined using quantitative real-time polymerase chain reaction (qRT-PCR) analysis. As shown in Fig. 3g, compared with mice without any treatment, the mice treated with direct illumination (80 mW cm^{-2}) exhibit a significant increase

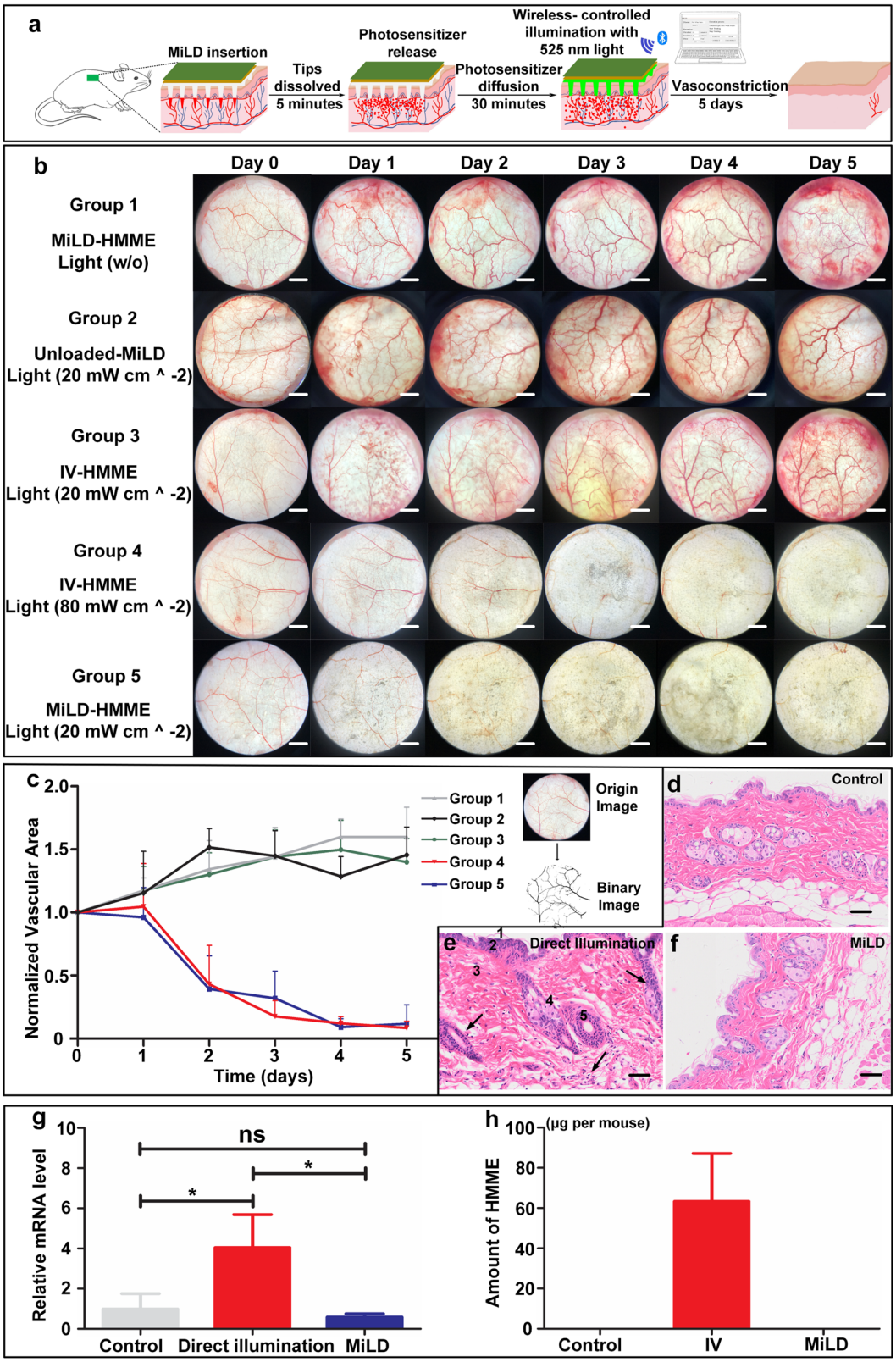

Fig. 3 | MiLD-mediated light therapy for removing disordered tissue in mice model. a Schematic diagram of utilizing MiLD-mediated PDT to treat PWS. **b** Vascular images of each group within 5 days after PDT. The decline of vascular area indicated efficient therapeutic effect (scale bar: 2 mm). **c** Quantitative analysis of vascular elimination in (**b**). **d**–**f** Representative images of hematoxylin and eosin (H&E) stained skin tissue treated with (**e**) direct illumination at 80 mW cm^{-2} irradiance and (**f**) MiLD emitting therapeutic light at 20 mW cm^{-2} irradiance. **d** Mice without any treatment acted as control (scale bar: 50 μm). Inflammatory cell infiltration (black arrows) was located in the skin tissue. 1, stratum corneum; 2, epidermis; 3, dermis; 4, sebaceous glands; 5, hair follicles. **g** Abnormal IL1 mRNA expressions induced by direct illumination at 80 mW cm^{-2} irradiance and MiLD emitting therapeutic light at 20 mW cm^{-2} irradiance. **h** Comparison of HMME plasma amount after MiLD application and intravenous administration. The data were presented as mean ± s.d.

Table 1 | Comparison between traditional PDT and MiLD-mediated PDT

		Traditional PDT LED-IE (China)	MiLD
Operation	Photosensitizer dosage [μg]	300	0.75
	Light irradiation [mW cm^{-2}]	80	20
	Therapeutic effect	92%	89%
	Shield light [day(s)]	More than 14	Not required
Device dimension	Volume [cm^3]	189,840	4.08
	Weight [kg]	22.5	0.0036

in the expressions of IL1 transcripts. The abnormal expressions are eliminated in mice treated with MiLD (20 mW cm^{-2}), avoiding the potential risk of overheating-induced inflammation.

In clinical PDT, intravenous injection results in a nonnegligible photosensitizer level in circulatory system, burdening metabolic organs or even causing systemic cytotoxicity for specific patients. Compared with intravenous injection, MiLD-mediated transdermal delivery remarkably reduces the amount of photosensitizer (MiLD: 0.75 μg HMME VS intravenous injection: 300 μg HMME for a single mouse), thus minimizing the photosensitizer level in circulatory system. HMME concentration in mice blood samples is measured by high performance liquid chromatography-triple quadrupole tandem type mass spectrometer (LC/MS/MS). The standard curve used to calculate HMME concentration is established as described in Supplementary Fig. 12. As shown in Fig. 3h, while intravenously injecting 300 μg HMME, 63.29 μg HMME is measured in blood 2 min after injection. In comparison, no HMME is detected while transdermally delivering 0.75 μg HMME by MiLD. The result suggests that MiLD eliminates circulatory photosensitizer. In summary, these findings suggest that MiLD significantly alleviates adverse effects in existing PDT, including therapeutic light-induced skin thermal damage and undesired photosensitizer accumulation in circulation.

In MiLD-mediated light therapy, the invasive damage mainly involves microneedle injection and therapeutic light irradiance. For microneedles invasive injection, microneedles are widely recognized as a minimally invasive strategy for transdermal drug delivery, which does not induce significant and long-term inflammatory responses or histological changes in the skin after injection. This technology has been successfully applied in various clinical areas, including vaccination and diabetes treatment, realizing a satisfactory therapeutic outcome with minimal adverse effects. Regarding therapeutic light irradiance, just as mentioned in Fig. 3f, MiLD-mediated light therapy employs a remarkably reduced light intensity (20 mW cm^{-2}) which does not significantly damage the skin, including histological change, skin inflammation, and abnormal expressions of mRNA. To comprehensively demonstrate the biosafety of MiLD, the co-influence of microneedle invasion and light irradiation on skin is investigated. As shown in Supplementary Fig. 13, MiLD has a satisfactory biocompatibility and safety profile and does not cause significant and persistent skin damage.

Overall, as listed in Table 1, compared with intra-hospital PDT with intravenous photosensitizer injection and direct illumination, MiLD-mediated PDT realizes similar therapeutic effect with a 400 times lower dosage of photosensitizer and 60% lower light irradiance, completely avoiding adverse effects. For instance, the photosensitizer accumulation in circulation and healthy skin tissue, which results in inconvenient shielding requirement, is fully eliminated. The therapeutic light-induced skin damage, including histological changes, skin inflammation, and abnormal expressions of mRNA, are also significantly alleviated. Moreover, from the equipment point of view, MiLD is a battery-powered fully portable device. The small size and lightweight features of MiLD are necessary to achieve point-of-care light therapy, not only enabling a timely response for acute diseases but also offering the possibility of relieving patients from the cumbersome and frequent commuting to the hospital while treating chronic diseases. The improved therapeutic effect and user-friendly operation of the MiLD technically lay the foundation of point-of-care light therapy.

MiLD-mediated light therapy for promoting the growth of healthy tissue

Light therapy may have broader application prospects in promoting normal tissue growth, compared with removing disordered tissue. For instance, photochemical tissue bonding (PTB), in which photosensitizers are light-activated to promote collagen cross-linking in wounds, has been gradually considered a promising technique for sutureless wound repair[39], a medical need that everyone may encounter. As a typical point-of-care scenario, wound repair raises high requirements for satisfactory therapeutic effects, minimized adverse effects, and more importantly, convenience of operation. These requirements cannot be fulfilled by existing intra-hospital light therapy equipment. The effectiveness of MiLD in performing PTB for wound repair is tested in mice. Figure 4a schemes a MiLD-mediated PTB operation for skin wound repair, involving 3 main steps. Firstly, three full-thickness incisions are made on the dorsal skin as a typical wound. Secondly, Rose Bengal (RB), a frequently used PTB photosensitizer, is loaded in needle tips of MiLD. After patching MiLD directly to the dorsal wound and maintaining it for several minutes, the needle tips are completely dissolved, releasing the photosensitizer to the wound. Thirdly, the MiLD is remotely commanded to emit therapeutic light at a wavelength of 525 nm, which is applied to the wound. After the PTB treatment, the skin incisions are expected to be immediately sealed. The wound repair process is monitored for 3 days. Mice are divided into 6 groups: Group 1 receives neither RB nor therapeutic light, exhibiting a natural recovery process of skin incisions. Group 2 receives unloaded-MiLD emitting therapeutic light, evaluating the effectiveness of applying light alone. Group 3 receives MiLD-mediated RB, but no therapeutic light is applied, demonstrating the influence of microneedles insertion. Groups 4 and 5, in which RB is directly smeared on the surface of skin incisions, receive direct illumination at 40 and 110 mW cm^{-2} irradiance, respectively. Group 6, in which both RB and therapeutic light are applied by MiLD, exhibits the therapeutic performance of MiLD. The skin incisions are photographed every day (Fig. 4b). In fact, a PTB-mediated wound healing consists of two main steps: immediate collagen crosslinks and tissue bonding-promoted wound healing. To accurately evaluate the performance of MiLD on PTB, the immediate bonding strength (Supplementary Fig. 14) after collagen crosslinks and the area of skin incisions demonstrating the wound healing process (Fig. 4c) are separately investigated. The bonding strength on day 0 is measured to evaluate the immediate collagen crosslinks. As shown in Supplementary Fig. 14, the skin incisions in Group 1 do not show immediate tissue bonding, with a bonding strength of only 0.009 N. Groups 2, 3, and 4 exhibit slightly higher incision bonding strength (0.188 N in Group 2, 0.208 N in Group 3 and 0.337 N in Group 4), while significantly higher incision bonding strength is observed in Groups 5 and 6. Higher bonding strength will promote wound healing, thus, the incisions area on day 3 is also measured to evaluate the final skin incisions healing outcome. As shown in Fig. 4c, significant incisions still exist in Group 1, with a skin incisions area being 0.421 cm^2, hinting that a 3-day period is not enough for natural incisions recovery. Skin incisions area in Groups 2 and 3 are 0.348 cm^2 and 0.365 cm^2, respectively. Similarly, the therapeutic effect of smearing RB and direct illumination at low irradiance (40 mW cm^{-2}, Group 4) is quite weak (0.3 cm^2), indicating the 40 mW cm^{-2} irradiance is not sufficient to facilitate skin incisions closure. By enhancing the irradiance from 40 to 110 mW cm^{-2}, the skin incisions area is decreased to 0.227 cm^2, realizing a satisfactory incisions healing effectiveness. However, just as mentioned in Fig. 3e, direct illumination at an irradiance higher than 80 mW cm^{-2} may induce tissue damage. In comparison, the MiLD-treated skin incisions show the smallest area (0.044 cm^2), with much lower irradiance (40 mW cm^{-2}), avoiding the high irradiance-induced skin damage. The experimental results demonstrate that MiLD facilitates an efficient and convenient point-of-care light therapy for promoting wound

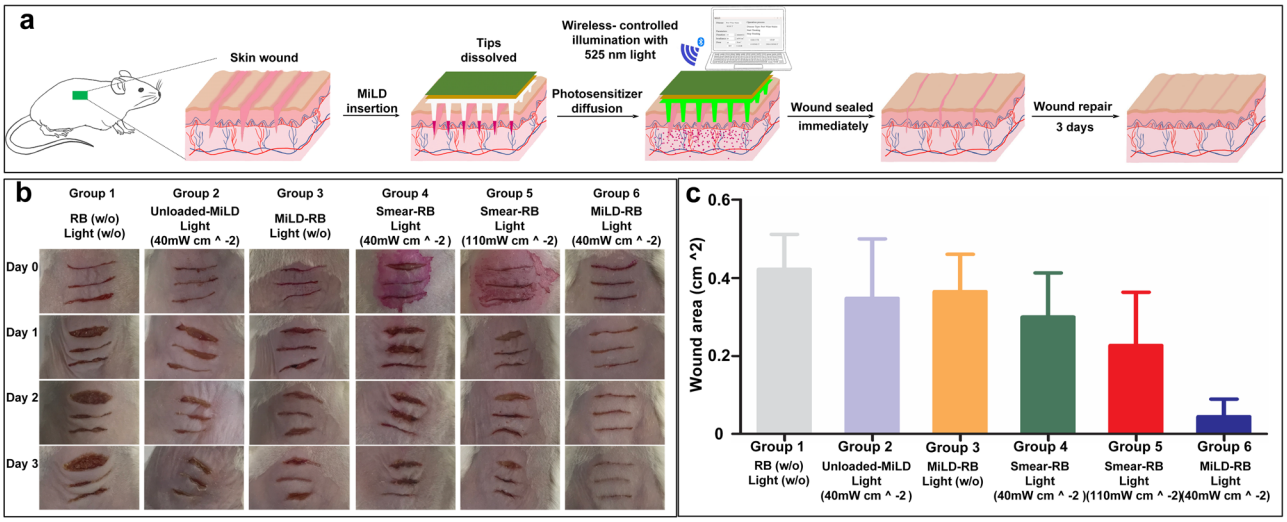

Fig. 4 | MiLD-mediated light therapy for promoting the growth of healthy tissue. **a** Schematic diagram of MiLD-mediated PTB for wound repair. **b** Wound images of each group within 3 days after treatment. Animals received the following treatments: (Group 1) mice without any treatment acted as control; (Group 2) mice were treated with unloaded MiLD, emitting therapeutic light; (Group 3) mice were treated with RB-loaded MiLD without therapeutic light; (Group 4) mice were smeared with RB and then illuminated at an irradiance of 40 mW cm^{-2}; (Group 5) mice were smeared with RB and then illuminated at an irradiance of 110 mW cm^{-2}; (Group 6) mice were treated with the RB-loaded MiLD emitting therapeutic light at an irradiance of 40 mW cm^{-2}. **c** The skin wound area of each group on 3rd day after treatment. The data were presented as mean ± s.d.

repair with significantly reduced light irradiance, avoiding possible therapeutic light-induced adverse effects. Apart from PDT-mediated PWS therapy and PTB-assisted wound healing, the MiLD can be modified to adapt to other light therapies. For instance, the light parameters of MiLD can be easily varied by changing the LEDs and driving circuit to facilitate aminolevulinic acid (MAL) or methyl aminolevulinic acid (ALA) based PDT, both of which require 630 nm wavelength. Moreover, the coverage area of the MiLD can be expanded by simply changing the design layout of the microneedle array.

Mainstream light therapies utilize the combined effects of photosensitizers and therapeutic light to treat diseases, especially superficial ones. However, multiple adverse effects have been reported in previous clinical studies, including harm to healthy tissue, metabolic burden caused by circulatory photosensitizer, and therapeutic light-induced skin damage. Meanwhile, bulky equipment and complex treatment procedures together restrict the employment of light therapy in central hospitals, compromising patient compliance, and more importantly, missing out on a broad range of point-of-care scenarios. This study provides a Miniaturized all-in-one Light therapy Device (MiLD) that facilitates efficient and convenient point-of-care light therapy with minimum adverse effects. Verified by mouse model, MiLD has demonstrated following prominent features: (i) The all-in-one design and patch-to-cure operation of MiLD enable the successful demonstration of point-of-care light therapy. (ii) Satisfactory therapeutic effects have been verified on both types of light therapy, including light-mediated disordered tissue removal and light-promoted healthy tissue growth. (iii) Transdermally co-delivering both photosensitizer and therapeutic light in situ fully avoids photosensitizer accumulation in blood and significantly reduces the irradiance of therapeutic light, therefore alleviating metabolic burden and therapeutic light-induced skin damage. Overall, MiLD lays the foundation of point-of-care light therapy with its miniaturized all-in-one design, simple patch-to-cure operation, satisfactory therapeutic effects and minimum adverse effects.

Methods

Materials

Sodium hyaluronate (HA) with a molecular weight of 7 KD (obtained from Nantong Feiyu Biological Technology Co., Ltd, China) was utilized in the preparation of the photosensitizer-loaded tips for the microneedle array. Polyvinyl alcohol (PVA) with a molecular weight of 70 KD (sourced from Sigma Aldrich, USA) was employed in fabricating the light-guiding bodies of the microneedle array. Polydimethylsiloxane (PDMS) (obtained from Dow Corning, USA) was selected for fabricating the microneedle mold. Hemoporfin (HMME) (obtained from Shanghai Fudan Zhangjiang Biomedical Co., Ltd, China) served as the photosensitizer for photodynamic therapy (PDT), while Rose Bengal (RB) (obtained from Sigma Aldrich, USA) functioned as the photosensitizer for photothermal therapy (PTB). Fluorescein isothiocyanate (FITC) (sourced from Sigma Aldrich, USA) was employed for assessing the depth of microneedle insertion into the mouse skin.

Animals

Female ICR mice weighing 30 g (obtained from Beijing Huafukang Biotechnology Co., Ltd, China) were housed under specific pathogen-free conditions. A dorsal skin-fold window chamber was surgically installed on the mouse to enable monitoring of the microvasculature. All animal experimental procedures were conducted in accordance with the guidelines and protocols approved by the Animal Experimental Ethics Committee of Beijing Institute of Technology (SYXK-BIT-20211118020).

Preparation of Miniaturized All-in-One Light Therapy Device (MiLD)

Figure 1o illustrated the process of fabricating MiLD. Before the fabrication of MiLD, all materials used to prepare the device, including the HA and PVA solution, LED light source, control module, and battery in MiLD, need to be sterilized by ultraviolet irradiation for 30 min. Firstly, a copper microneedle master (900 μm in height, 300 μm in width, 500 μm in spacing, and 20 × 20 array), was created using a machine tool (JDPGT600, Beijing Jingdiao Technology Group Co., Ltd, China). The Polydimethylsiloxane (PDMS) (a mixture of Sylgard 184 silicone elastomer and curing agent in a 10:1 w/w ratio) was poured on the master and then cured at 80 °C for 30 min. The PDMS mold was created by peeling off the master carefully. The HA-water solution (0.2 g ml^{-1}) was prepared, and then photosensitizer was added to the HA-water solution to create the photosensitizer-loaded HA solution. Furthermore, PVA was dissolved in distilled water to generate PVA solution (15% (w/v)). The photosensitizer-loaded HA solution (0.1 ml) was applied to the PDMS mold. The mold was placed in a vacuum environment (−0.9 bar) for 30 min, and then the excess solution remaining on the surface was cleared. The PVA-water solution was applied to the PDMS mold and

the mold was placed in the same vacuum environment for 10 min to fabricate the light-guiding needle bodies beneath the HA tips. The polyvinyl alcohol (PVA) solution had not yet solidified during this phase. The LED array, with a wavelength of 525 nm, was firmly affixed to the PVA solution and remained in place until the PVA fully solidified over a period of 48 h at room temperature. The base width and height of the PVA needle body are 300 and 700 μm, respectively. The height of the HA needle tip is 100 μm. Hence, the total height of a microneedle is 800 μm. Subsequently, the LED-coupled microneedle array was delicately removed from the polydimethylsiloxane (PDMS) mold once it had completely dried. Finally, the graphene membrane, control module, and battery were sequentially assembled onto the back of the LED-coupled microneedle array to construct the MiLD.

To assess the microneedle array, it underwent examination and characterization using a stereoscope from Keyence, Japan. The sizes of the microneedles were measured. Additionally, after applying a thin layer of gold to the microneedles surface, scanning electron microscopy (SEM) from Zeiss, Germany, was employed for high-resolution imaging purposes.

Transdermal photosensitizer delivery of microneedle array

To evaluate the depth of photosensitizer delivery following microneedle insertion into the skin, FITC-loaded MiLD was inserted into the mice. Subsequently, full-thickness skin samples were collected, ensuring the removal of excess subcutaneous fat and connective tissue. These excised skin samples were then placed on glass slides and subjected to examination using a confocal laser scanning microscope (Nikon, Japan). The FITC signal intensity within the skin was detected under 488 nm excitation wavelength and 520 nm emission wavelength. Images were captured in the skin surface, which was designated as the imaging plane starting to show fluorescence. Scanning was performed at 20 μm intervals along the z-axis, which was perpendicular to the skin surface, allowing for precise assessment of the depth of FITC penetration into the skin.

Simulation of light guide

Three Monte Carlo simulations were used to illustrate the light distribution within the skin. In the first simulation, the light irradiance was set at 20 mW cm^{-2} in the presence of the microneedles. (microneedles-mediated illumination). In the second simulation, the light irradiance was set at 20 mW cm^{-2} in the absence of the microneedles (direct illumination, DI). In the third simulation, the light irradiance was set at 80 mW cm^{-2} in the absence of the microneedles. The thickness of the stratum corneum, epidermis, and dermis were 20 μm, 30 μm, and 150 μm respectively. The optical parameters including refractive index, absorption coefficient, scattering coefficient, and anisotropy factor were listed in Supplementary Table 1.

In vivo photodynamic therapy

To evaluate the effectiveness of MiLD-mediated light therapy in removing disordered tissue, female ICR mice were randomly divided into five groups ($n = 6$): (1) Group 1, mice were treated with HMME-loaded MiLD (0.75 μg HMME), without therapeutic light. (2) Group 2 ($n = 3$), mice were treated with unloaded MiLD, emitting therapeutic light at an irradiance of 20 mW cm^{-2} for 15 min. (3) Group 3, mice were intravenously injected (IV) with HMME (300 μg), and then directly illuminated with therapeutic light at an irradiance of 20 mW cm^{-2} for 15 min after 5 min post-administration. (4) Group 4, mice were intravenously injected with HMME (300 μg), and then directly illuminated with therapeutic light at an irradiance of 80 mW cm^{-2} for 15 min after 5 min post-administration. (5) Group 5, mice were treated with HMME-loaded MiLD (0.75 μg HMME), emitting therapeutic light at an irradiance of 20 mW cm^{-2} for 15 min after 30 min post-administration. The therapeutic effect was evaluated by measuring change in the vascular area.

Histopathological analysis

To evaluate the histological changes and inflammation, mice were randomly divided into three groups ($n = 1$): Control group, the mice without any treatment. (2) Direct illumination group, mice were directly illuminated with therapeutic light at an irradiance of 80 mW cm^{-2} for 15 min. (3) MiLD illumination group, mice were treated with MiLD, emitting therapeutic light at an irradiance of 20 mW cm^{-2} for 15 min. The mice were sacrificed after 24 h, and the irradiated skin (about 1 cm^2 in size) were dissected. The skin samples were fixed with 4% paraformaldehyde and then embedded in paraffin. The serial sections were stained by a published hematoxylin and eosin (H&E) procedure. The slides were observed by Research Slide Scanner.

Quantitative real-time PCR analysis

Female ICR mice were randomly divided into three groups ($n = 3$) and the procedures were as same as described above. Mice were sacrificed after 24 h illumination and the irradiated skin were dissected. mRNA was extracted from skin tissue using the Gene JET RNA Purification Kit (Thermo Fisher, USA). cDNA was obtained by reverse transcriptase using the SuperScript First-Strand cDNA Synthesis SuperMix (Transgen Biotech, China). Quantitative real-time PCR was performed using the 7500 Real-Time PCR System (Thermo Fisher, USA) in a mixture containing cDNA, SYBR Green Master Mix (Genstar, China) and specific primer pair (Sangon Biotech, China). The specific primer sequences for mouse IL1 and GAPDH were listed in Supplementary Table 2. The cycling programs involved an initial step at 95 °C for 10 min, followed by 40 cycles of 95 °C for 15 s and 60 °C for 45 s. To control variation in mRNA concentration, all results were normalized to the housekeeping gene, GAPDH. Relative quantitation was performed using the comparative ΔΔCt method.

Pharmacokinetic study

Female ICR mice were randomly divided into three groups ($n = 6$): (1) Control group, mice without any treatment. (2) IV-HMME group, mice were intravenously injected with HMME (300 μg). (3) MiLD-HMME group, mice were treated with HMME-loaded MiLD (0.75 μg HMME). After administration, blood (400 μl) was collected and extracted with methanol (900 μl). The mixture was centrifuged (15,000 rpm) for 15 min and the supernatant was collected for analysis. The amount of HMME in blood was determined using high performance liquid chromatography-triple quadrupole tandem type mass spectrometer (LC/MS/MS) (Thermo Fisher, USA). The separation was achieved using Ultimate UHPLC XB-C18 (Yuexu Technology Co., Ltd, China). The mobile phase consisted of methanol/water (a ratio of 85/15), and the flow rate was 0.2 ml min^{-1}.

In vivo photochemical tissue bonding

To evaluate the effectiveness of MiLD-mediated light therapy in promoting the growth of healthy tissue, mice were divided into six groups ($n = 3$). Three incisions (1 cm) were made on the dorsal skin: Group 1, mice without any treatment, acted as the control. Group 2, mice were treated with unloaded MiLD emitting therapeutic light at irradiances of 40 mW cm^{-2} for 20 min. Group 3, mice were treated with Rose Bengal (RB)-loaded MiLD (22.5 μg RB) without therapeutic light. Groups 4 and 5, mice were topically smeared with RB (0.05% (w/v)) and then directly illuminated with therapeutic light at irradiances of 40 and 110 mW cm^{-2} for 20 min, respectively. Group 6, mice were treated with RB-loaded MiLD (22.5 μg RB), emitting therapeutic light at an irradiance of 40 mW cm^{-2} for 20 min. Incisions on the back of mice were observed on days 0, 1, 2, and 3 post-treatment, and incisions area was measured and analyzed on day 3 using Image J. Treated skin (1×2.5 cm^2) was collected at day 0 for bonding strength testing. The force required to reopen the wound incisions (bonding strength) was measured using a universal testing machine (Wenzhou Pinuo Instrument Co., Ltd, China) equipped with a load cell (weight in 10 N). The treated skin was loaded on universal testing machine and slowly pulled until the two incisions were completely separated. The data from the samples were averaged to calculate the bonding strength.

Statistical analysis

Statistical analysis was conducted using a two-tailed unpaired Student's t test in GraphPad Prism (GraphPad Software, USA). Data were presented as

mean ± standard deviation (SD). The comparisons between groups were considered statistically significant if $p < 0.05$.

Data availability

The data that support findings of this study are available from the corresponding author upon reasonable request.

Received: 4 November 2023; Accepted: 11 May 2024;
Published online: 28 May 2024

References

1. Finsen, N. R. *Phototherapy: 1. The chemical rays of light and smallpox, 2. Light as a stimulant, 3. The treatment of lupus vulgarisby concentrated chemical rays* (Arnold, 1901).
2. Vieyra-Garcia, P. A. & Wolf, P. A deep dive into UV-based phototherapy: mechanisms of action and emerging molecular targets in inflammation and cancer. *Pharmacol. Ther.* **222**, 107784 (2021).
3. Armstrong, A. W. & Read, C. Pathophysiology, clinical presentation, and treatment of psoriasis: a review. *JAMA* **323**, 1945–1960 (2020).
4. Migayron, L., Boniface, K. & Seneschal, J. Vitiligo, from physiopathology to emerging treatments: a review. *Dermatol. Ther.* **10**, 1185–1198 (2020).
5. Musters, A. H. et al. Phototherapy for atopic eczema. *Cochrane Database Syst. Rev.* **10**, Cd013870 (2021).
6. Yun, S. H. & Kwok, S. J. J. Light in diagnosis, therapy and surgery. *Nat. Biomed. Eng.* **1**, 0008 (2017).
7. Zhao, X., Li, X., Zhang, P., Du, J. & Wang, Y. Tip-loaded fast-dissolving microneedle patches for photodynamic therapy of subcutaneous tumor. *J. Control. Release* **286**, 201–209 (2018).
8. Nicolo, M., Desideri, L. F., Vagge, A. & Traverso, C. E. Current pharmacological treatment options for central serous chorioretinopathy: a review. *Pharmaceuticals* **13**, 264 (2020).
9. Braathen, L. R. et al. Short incubation with methyl aminolevulinate for photodynamic therapy of actinic keratoses. *J. Eur. Acad. Dermatol. Venereol.* **23**, 550–555 (2009).
10. Huang, Y., Yang, J., Sun, L., Zhang, L. & Bi, M. Efficacy of influential factors in hemoporfin-mediated photodynamic therapy for facial port-wine stains. *J. Dermatol.* **48**, 1700–1708 (2021).
11. Sheleg, S. V. et al. Photodynamic therapy with chlorin e(6) for skin metastases of melanoma. *Photodermatol. Photo* **20**, 21–26 (2004).
12. Feng, Y. et al. Assembly of upconversion nanophotosensitizer in vivo to achieve scatheless real-time imaging and selective photodynamic therapy. *Biomaterials* **201**, 33–41 (2019).
13. Chen, D. et al. Photothermal-pH-hypoxia responsive multifunctional nanoplatform for cancer photo-chemo therapy with negligible skin phototoxicity. *Biomaterials* **221**, 119422 (2019).
14. Li, X. et al. A tumor-pH-responsive supramolecular photosensitizer for activatable photodynamic therapy with minimal in vivo skin phototoxicity. *Theranostics* **7**, 2746–2756 (2017).
15. Glickman, R. D. Ultraviolet phototoxicity to the retina. *Eye. Contact Lens.* **37**, 196–205 (2011).
16. Dougherty, T. J., Cooper, M. T. & Mang, T. S. Cutaneous phototoxic occurrences in patients receiving Photofrin. *Lasers Surg. Med.* **10**, 485–488 (1990).
17. Henderson, B. W. et al. Photofrin photodynamic therapy can significantly deplete or preserve oxygenation in human basal cell carcinomas during treatment, depending on fluence rate. *Cancer Res.* **60**, 525–529 (2000).
18. Han, S. et al. Upconversion nanoparticles/hyaluronate-rose bengal conjugate complex for noninvasive photochemical tissue bonding. *Acs. Nano.* **11**, 9979–9988 (2017).
19. Wang, X., Xiong, J., Hu, X. & Li, Q. Implementation and uniformity calibration of LED array for photodynamic therapy. *J. Innov. Opt. Heal. Sci.* **15**, 224000 (2022).
20. Keller, A., Hartmann, J., Enk, A. & Gholam, P. Pulse rate and blood pressure changes during low-irradiance PDT compared with conventional PDT in the treatment of facial actinic keratoses: a retrospective study. *Photodermatol. Photoimmunol. Photomed.* **38**, 435–441 (2022).
21. Clydesdale, G. J., Dandie, G. W. & Muller, H. K. Ultraviolet light induced injury: immunological and inflammatory effects. *Immunol. Cell. Biol.* **79**, 547–568 (2001).
22. Petersen, B., Wiegell, S. R. & Wulf, H. C. Light protection of the skin after photodynamic therapy reduces inflammation: an unblinded randomized controlled study. *Br. J. Dermatol.* **171**, 175–178 (2014).
23. O'Mahoney, P. et al. A novel light source with tuneable uniformity of light distribution for artificial daylight photodynamic therapy. *Photodiagnos. Photodyn. Ther.* **23**, 144–150 (2018).
24. Kim, M. M. & Darafsheh, A. Light sources and dosimetry techniques for photodynamic therapy. *Photochem. Photobiol.* **96**, 280–294 (2020).
25. Yu, N. et al. Dermabrasion combined with photodynamic therapy: a new option for the treatment of non-melanoma skin cancer. *Lasers Med. Sci.* **37**, 1255–1263 (2022).
26. Ferrara, F. et al. Combined CO_2 laser and photodynamic therapy enhances the efficacy of treatment of basal cell carcinomas. *J. Dtsch. Dermatol. Ges.* **17**, 1251–1256 (2019).
27. Portugal, I., Jain, S., Severino, P. & Priefer, R. Micro- and nano-based transdermal delivery systems of photosensitizing drugs for the treatment of cutaneous malignancies. *Pharmaceuticals* **14**, 772 (2021).
28. Risaliti, L. et al. Topical formulations of delta-aminolevulinic acid for the treatment of actinic keratosis: Characterization and efficacy evaluation. *Eur. J. Pharm. Sci.* **115**, 345–351 (2018).
29. Pivetta, T. P. et al. Liposomes encapsulating methylene blue and acridine orange: an approach for phototherapy of skin cancer. *Colloids Surf. B. Biointerfaces* **220**, 112901 (2022).
30. Lemos, C. N., de Souza, J. G., Simão, P. S. & Lopez, R. F. Iontophoresis improved growth reduction of invasive squamous cell carcinoma in topical photodynamic therapy. *PLoS. One* **11**, e0145922 (2016).
31. Liu, F., Cheng, Z. & Yi, H. NIR light-activatable dissolving microneedle system for melanoma ablation enabled by a combination of ROS-responsive chemotherapy and phototherapy. *J. Nanobiotechnol.* **21**, 61 (2023).
32. Choi, S. H., Kim, T. H. & Song, K. H. Efficacy of iontophoresis-assisted ablative fractional laser photodynamic therapy with short incubation time for the treatment of actinic keratosis: 12-month follow-up results of a prospective, randomised, comparative trial. *Photodiagnos. Photodyn. Ther.* **18**, 105–110 (2017).
33. Petukhova, T. A., Hassoun, L. A., Foolad, N., Barath, M. & Sivamani, R. K. Effect of expedited microneedle-assisted photodynamic therapy for field treatment of actinic keratoses: a randomized clinical trial. *Jama. Dermatol.* **153**, 637–643 (2017).
34. Fadel, M., Samy, N., Nasr, M. & Alyoussef, A. A. Topical colloidal indocyanine green-mediated photodynamic therapy for treatment of basal cell carcinoma. *Pharm. Dev. Technol.* **22**, 545–550 (2017).
35. Nizamoglu, S. et al. Bioabsorbable polymer optical waveguides for deep-tissue photomedicine. *Nat. Commun.* **7**, 10374 (2016).
36. Zhang, H. et al. Biocompatible light guide-assisted wearable devices for enhanced UV light delivery in deep skin. *Adv. Funct. Mater.* **31**, 2100576 (2021).
37. Zhao, H. et al. Dual-function microneedle array for efficient photodynamic therapy with transdermal co-delivered light and photosensitizers. *Lab Chip* **22**, 4521–4530 (2022).
38. Zhang, L. C., Yang, J., Huang, Y. B. & Bi, M. Y. Efficacy of hemoporfin photodynamic therapy for pulsed dye laser-resistant facial port-wine stains in 107 children: a retrospective study. *Indian. J. Dermatol. Venereol. Leprol.* **88**, 275 (2022).

39. Ark, M., Cosman, P. H., Boughton, P. & Dunstan, C. R. Review: photochemical tissue bonding (PTB) methods for sutureless tissue adhesion. *Int. J. Adhes. Adhes.* **71**, 87–98 (2016).

Acknowledgements

This work was supported by the National High Technology Research and Development Program of China (No. 2022YFC2403301), the National Natural Science Foundation of China (No. 62074016), the Frontier Interdisciplinary Innovation Project of Beijing Institute of Technology (2023CX11011), the Laboratory Funding of the National Key Laboratory of Science and Technology on Micro/Nano Fabrication (No.6142805200104), the Quancheng-5150 Talent Supporting Project of Jinan (Laureate, Zewen Wei) and the Industrial Talent Supporting Project of Huaiying (Laureate, Zewen Wei). We thanked the Biological & Medical Engineering Core Facilities of Beijing Institute of Technology and the Analysis & Testing Center of Beijing Institute of Technology for characterization services. We thanked the Department of Dermatology, Beijing Tsinghua Changgung Hospital, and School of Clinical Medicine, Tsinghua University, Beijing, China for providing the HMME.

Author contributions

H.T.Z. and X.W. contributed equally to this work. H.T.Z., X.W. and Z.W.W. together conceived and designed the experiment. Z.W.W. and X.M.H. supervised the project. H.T.Z. and X.W. conducted most of the experiments. J.Y.X., G.M.L., X.W. and J.Y.X. analyzed the experimental data and explained the results. Y.Z. and Z.X.L. carried out theoretical simulations and analyzed the data. Z.W.W. and H.T.Z. wrote the manuscript with contributions from all the authors. All authors reviewed the manuscript.

Competing interests

The authors declared no competing interests.

Additional information

Supplementary information The online version contains supplementary material available at https://doi.org/10.1038/s41528-024-00317-z.

Correspondence and requests for materials should be addressed to Xiaoming Hu or Zewen Wei.